ACS APPLIED MATERIALS & INTERFACES

Research Article

www.acsami.org

# Charge Transport Across High Surface Area Metal/Diamond Nanostructured Composites

D. Plana,[†] J. J. L. Humphrey,[†] K. A. Bradley,[†,‡] V. Celorrio,[†] and D. J. Fermín*,[†]

[†]School of Chemistry, University of Bristol, Cantocks Close, Bristol BS8 1TS, U.K.

[‡]Bristol Centre for Functional Nanomaterials, NSQI Building, University of Bristol, Tyndall Avenue, Bristol BS8 1FD, U.K.

**ABSTRACT:** High surface area composites featuring metal nanostructures and diamond particles have generated a lot of interest in the fields of heterogeneous catalysis, electrocatalysis, and sensors. Diamond surfaces provide a chemically robust framework for active nanostructures in comparison with $sp^2$ carbon supports. The present paper investigates the charge transport properties of high surface area films of high-pressure, high-temperature diamond particles in the presence and absence of metal nanostructures, employing electrochemical field-effect transistors. Oxygen- and hydrogen-terminated surfaces were generated on 500 nm diamond powders. Homogeneously distributed metal nanostructures, with metal volume fractions between ca. 5 and 20%, were either nucleated at the diamond particles by impregnation or incorporated from colloidal solution. Electrochemical field-effect transistor measurements, employing interdigitated electrodes, allowed the determination of composite conductivity as a function of electrode potential, as well as in air. In the absence of metal nanostructures, the lateral conductivity of the diamond assemblies in air is increased by over one order of magnitude upon hydrogenation of the particle surface. This observation is consistent with studies at diamond single crystals, although the somewhat modest change in conductivity suggests that charge transport is not only determined by the intrinsic surface conductivity of individual diamond particles but also by particle-to-particle charge transfer. Interestingly, the latter contribution effectively controls the assembly conductivity in the presence of an electrolyte solution as the difference between hydrogenated and oxygenated particles vanishes. The conductivity in the presence of metal nanoparticles is mainly determined by the metal volume fraction, while diamond surface termination and the presence of electrolyte solutions exert only minor effects. The experimental trends are discussed in terms of the electrochemical formation of charge carriers in the diamond particles, percolation theory, and charge screening at the double layer.

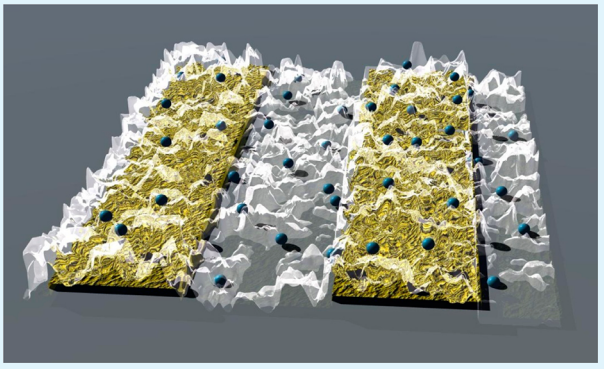

**KEYWORDS:** *high-pressure high-temperature nanodiamond, nanoparticles, nanocomposites, charge transport, percolation theory*

## 1. INTRODUCTION

In recent years, small diamond particles have been generating considerable interest as highly stable platforms for active systems in catalysis and sensing applications.[1−4] Diamond particles obtained by either detonation or high-pressure, high-temperature methods are essentially insulators; however, distinct redox properties have been reported when assembled at electrode surfaces.[5−7] This redox activity could have multiple origins, such as surface functional groups (carboxylic acid, ether, lactone, hydroxyl, and ketone) or the generation of holes in the valence band of diamond. The latter mechanism has been observed in hydrogen-terminated crystalline powders,[7] which is consistent with the so-called transfer doping model observed in extended non-boron-doped diamond films.[8] These properties pave the way for exploiting diamond particles in many new and exciting applications, particularly in the areas of life sciences and electronics.[9−12] However, unlike the well-established electrochemical properties of boron-doped diamond films,[13−15] fundamental questions with regards to the dynamics of charge transport in assemblies of diamond particles remain unaddressed.

Composite materials featuring small diamond particles as support for metallic nanostructures have also been considered as electrocatalysts for fuel cell applications.[16−18] In principle, this approach provides a solution for the corrosion of carbon black commonly employed as a catalyst support.[19] So far, it is unclear how charges are transported in these complex assemblies and whether diamond particles actively participate in the transport mechanism. In this work, we investigate for the first time the dynamics of charge transport in metal/diamond composites in air, as well as in an electrochemical environment, employing electrochemical field-effect transistors. This approach is based on interdigitated electrodes with potentials individually controlled by a bi-potentiostat.[20] Pd-based nanostructures are incorporated into hydrogen- and oxygen-

Received: October 19, 2012
Accepted: March 19, 2013
Published: March 19, 2013

   dx.doi.org/10.1021/am302397p | ACS Appl. Mater. Interfaces 2013, 5, 2985−2990

terminated diamond particles by two different methods, ensuring that the preparation of the metal/diamond composite does not compromise the initial surface termination of the diamond support. Systematic measurement of the lateral conductivity of the assemblies allowed unraveling contributions from: (i) the intrinsic surface conductivity of the diamond support, (ii) particle-to-particle charge transport, (iii) charge percolation paths created by the metallic nanostructures, and (iv) the role of ionic species in the electrochemical environment.

## 2. EXPERIMENTAL SECTION

High-pressure, high-temperature type Ib diamond particles featuring a 500 nm nominal size (Microdiamant AG-MSY005) were employed as the base material for the composites. These particles have a significantly higher degree of crystallinity, lower content of carbon $sp^2$ impurities, and lower tendency to agglomerate than detonated diamond nanoparticles. These are key advantages for investigating subtle effects associated with surface termination. However, it should be recognized that the specific surface area of this diamond material, 10.7 $m^2\ g^{-1}$ as estimated from BET isotherms, is significantly smaller than carbon black powders conventionally used in electrocatalysis. Surface groups have been shown to be of paramount importance on the electrochemical properties of diamond,[5,8,9,21] and consequently the diamond particles were treated to modify their surface, obtaining both oxygen- and hydrogen-terminated diamond particles.[7] The as-received particles were sonicated in ultrapure water and subsequently heated to 200 °C in a mixture of concentrated $H_2SO_4$ and $HNO_3$ (9:1, v/v) for 30 min to remove impurities and produce oxygen surface groups. After the acid bath, the oxygen-terminated diamond particles (ODP) were thoroughly washed with Milli-Q water and separated by centrifuge until the supernatant became pH neutral. In order to create hydrogen-terminated diamond particles (HDP), ODP were introduced, twice stirring at room temperature in between sessions, in an 800 W microwave plasma reactor with a hydrogen flow rate of 500 sccm and a pressure of 50 Torr for 2 min.

Two methods were employed for generating Pd/diamond composites as shown in Table 1. Method 1 involves impregnation of diamond powders (80 mg) with a solution of sodium hexachloropalladate(IV) tetrahydrate (84 mg in 35 mL of ultrapure water) followed by reduction with sodium borohydride (20 mg in 20 mL).[16] This procedure was implemented in hydrogen- and oxygen-terminated diamond powders, yielding composites labeled as M1-HDP and M1-ODP, respectively. Method 2 consists of suspending each diamond powder (23 mg) in colloidal Au–Pd core–shell nanoparticle solution (9 mg in 40 mL) under strong stirring for 48 h. The synthesis of the Au–Pd core–shell nanoparticles involves the reduction of $H_2PdCl_4$ into 20 nm Au cores in the presence of ascorbic acid.[22] Detailed structural analysis of the core–shell nanostructures employing high-resolution transmission electron microscopy, selected area electron diffraction, and X-ray diffraction (XRD) has been published elsewhere.[22−24] The fact that no metal reduction step is involved in Method 2 ensures that no changes are induced in the surface termination of the diamond particles during composite preparation. The as-prepared composites were filtered or centrifuged, washed with Milli-Q water, and dried at 60 °C overnight. The core–shell nanostructures and all metal/diamond composites were fully characterized by X-ray diffraction and various electron microscopy techniques.

**Table 1. Preparation of Pd–Diamond Composites**

| | preparation | composite[a] |
|---|---|---|
| Method 1 | Impregnation of diamond powders (80 mg) with $Na_2PdCl_6$ (80 mg/35 mL) followed by reduction with $NaBH_4$ (20 mg/20 mL) | M1-HDP<br>M1-ODP |
| Method 2 | Suspension of diamond powders (23 mg) and Au–Pd core–shell nanoparticles (9 mg/40 mL) | M2-HDP<br>M2-ODP |

[a]HDP: Hydrogen-terminated diamond powder. ODP: Oxygen-terminated diamond powder.

Elemental composition, metal loading, and elemental mapping of the different metal/diamond composites were determined by energy-dispersive X-ray spectroscopy (EDX), using a JEOL 5600LV scanning electron microscope (SEM) coupled with an Oxford Instruments 'ISIS 300' system. The dispersion of the Pd@Au nanoparticles on each of the diamond supports was also assessed by images obtained with a field-emission gun SEM. Size and composition of the diamond supported metallic nanoparticles were measured by XRD at room temperature using Cu K$\alpha$ radiation (40 kV, 40 mA) with a Bruker AXS Advance D8 diffractometer.

Electrochemical measurements were carried out using an Ivium bipotentiostat equipped with IviumSoft software. Measurements were performed in a 0.5 M $H_2SO_4$ electrolyte, with a Pt foil counter electrode and a $Ag/AgCl_{sat}$ reference electrode. Droplets (20 $\mu$L) of an ink prepared for each sample were drop-cast onto glassy carbon disks or gold interdigitated microsensor electrodes and dried in air prior to measurements. Inks were made from the diamond composites (2.0 mg) using Nafion (15 $\mu$L of a 10% aqueous dispersion) and water (0.5 mL). The metal/diamond composites were electrochemically pretreated by at least 50 cycles between −0.35 and 1.0 V, at 500 mV $s^{-1}$. Previous studies have shown that Pd and Au–Pd nanostructures are stable in this potential range.[16,23,24]

The cell configuration used for the electrochemical field-effect transistor experiments is illustrated in Figure 1.[20] As mentioned earlier,

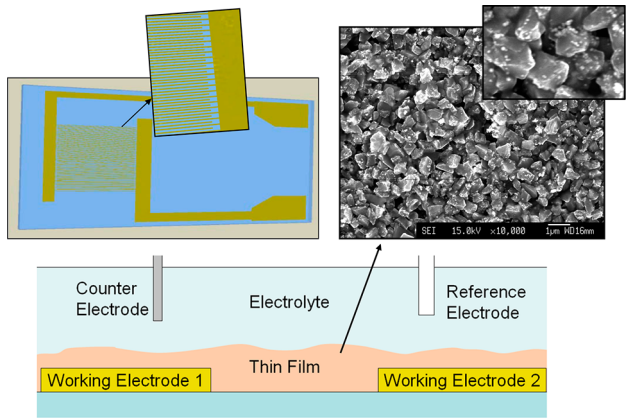


**Figure 1.** Schematic representation of the Au interdigitated microsensor electrode (on a 2 × 1 $cm^2$ glass substrate), featuring 50 pairs of digits 20 $\mu$m × 5 mm, with 20 $\mu$m gaps. The bottom diagram depicts the electrochemical field effect transistor configuration used, where working electrodes 1 and 2 act as source and drain. The SEM image displays a typical M2-HDP composite (Method 2).

Au interdigitated electrodes (IME 2050.5-M-Au-U, ABTECH Scientific) were covered with each of the composites and introduced in the electrolyte solution. The potential of each electrode (with respect to the reference electrode) in the interdigitated microsensor was controlled by a bi-potentiostat system. The experimental approach involved setting a potential at the interdigitated electrodes (gate voltage, $E_{gate}$), within the capacitive region obtained from cyclic voltammetry, and allowing the current to relax to zero. At this point, a small potential offset was applied between the two terminals of the interdigitated microsensor electrode (source–drain voltage, $E_{sd}$), and the source–drain current ($I_{sd}$) was allowed to stabilize (360 s). Ohmic behavior is observed for $E_{sd}$ in the range of −25 to 25 mV, from which the film conductance is estimated as a function of $E_{gate}$. The film conductivity was calculated from the conductance, taking into account the interdigitated microsensor electrode cell constant (0.04 $cm^{-1}$). It should be emphasized that this approach is only valid in the potential range where no faradaic reaction takes place (i.e., charge transfer resistance is infinitely larger than the composite resistance). Finally,

conductivity in air was measured using a conventional two-electrode system (the two terminals of the interdigitated microsensor) by sweeping the potential between −0.45 and 0.45 V at 1 mV $s^{-1}$.

## 3. RESULTS AND DISCUSSION

**3.1. Composite Characterization.** The scanning electron micrograph in Figure 1 illustrates the structure of composites prepared by Method 2 (incorporation of nanoparticles onto a hydrogen-terminated diamond). The diamond particles are characterized by sharp edges, typical of high-pressure, high-temperature growth. The 43 nm core−shell particles can be observed dispersed through the composite with only a few aggregates. In all cases, these aggregates are significantly smaller than the size of the diamond particles. Composites obtained by impregnation (Method 1) produced significantly smaller Pd nanoparticles, which could not be clearly identified by SEM.

Topographic SEM studies combined with elemental mapping of composites produced by both methods are contrasted in Figure 2. The top panels show the main topographic features

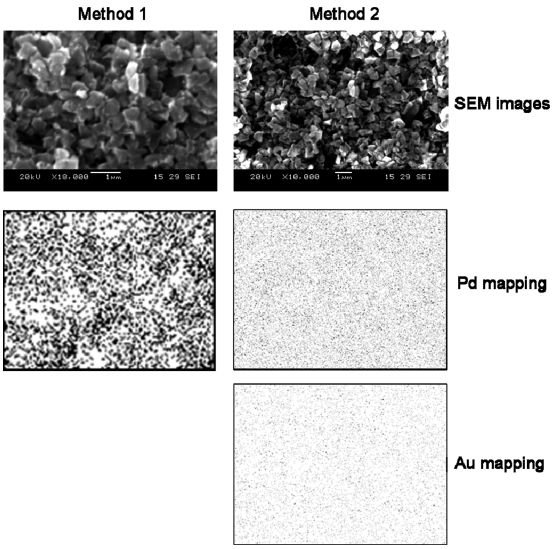


**Figure 2.** SEM images of Pd-impregnated diamond powders (Method 1) and nanoparticle-loaded diamond powders (Method 2). Au−Pd core−shell nanostructures were employed in Method 2. The second row of panels shows Pd elemental mapping on the samples, while the last image represents the distribution of Au cores on the composite obtained by Method 2.

associated with the diamond particles, while the dispersion of the metallic particles is visible through the elemental mapping shown on the lower panels. It is clear that the metal is homogeneously dispersed over the composites in both cases. Furthermore, the similar distribution of Au and Pd observed in composites obtained via Method 2 confirmed that the core−shell structure is not compromised during preparation.

TEM of the particles, prior to incorporation on the diamond, confirmed the core−shell nature and allowed the determination of the diameter of the particles; the size of the Au cores and the thickness of the Pd layer were also determined, as shown in Table 2.[23] It can be seen that Method 1 produces smaller particles than those used in Method 2. There is a difference in Pd particle size and loading between the HDP and ODP, likely due to the different nucleation sites for metal deposition on the diamond surface. Method 2, on the other hand, produced, within experimental error, similar metal loading.

**Table 2. Metal Loading (Weight Percentage), Volume Fraction and Nanoparticle Diameter ($d$), of the Various Diamond Composites**

| composite | metal loading (%) | $d$/nm | metal volume fraction |
|---|---|---|---|
| M1-ODP | 31 ± 2.1 | 10 | 0.12 |
| M1-HDP | 43 ± 1.8 | 7 | 0.18 |
| M2-ODP | 19 ± 2.3 | 43 (Au core: 19 nm; Pd overlayer: 12 nm) | 0.06 |
| M2-HDP | 23 ± 2.4 | | 0.08 |

X-ray diffraction patterns confirmed the polycrystalline nature of the Pd and core−shell nanoparticles. Figure 3

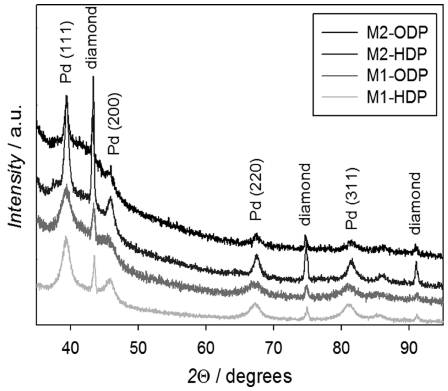


**Figure 3.** XRD patterns of the different metal/diamond composites.

shows XRD patterns obtained for the various metal/diamond composites. The sharp, well-defined peaks at $2\theta$ = 43.3, 74.7, and 91.1 are indicative of the highly crystalline structure of the diamond particles. The additional peaks at $2\theta$ values of 39.4, 45.6, 67.4, and 81.3 are associated with the (111), (200), (220), and (311) Pd planes, respectively. The average Pd crystal size produced by Method 1 was estimated by the Scherrer equation employing the (111) and (200) reflections (see Table 2). The broadening of the XRD peaks associated with the Au core is consistent with the 19 nm diameter estimated from transmission electron microscopy studies reported elsewhere.[22,24]

As shown in Table 2, energy-dispersive X-ray (EDX) spectroscopy was used to determine the overall metal loading of each composite; the Pd:Au mass ratio obtained was consistent with that calculated using the dimensions obtained through TEM. Method 1 produced higher and more varied metal loadings, again the diamond surface having an influence over the metal particle growth, which is absent in Method 2.

Knowing the density of each of the elements involved (Au, Pd, and diamond depending on the sample), metal loadings were transformed into volume fractions of metal for each metal/diamond composite. It should be clarified that this approach did not consider the free volume within the network of irregularly shaped hard diamond particles; i.e., it was assumed the composites consisted solely of diamond and metal, with no free spaces. The values obtained are presented in Table 2, and it can be seen that the metal volume fraction of the impregnated samples is approximately twice that of the equivalent core−shell sample. As discussed below, this parameter affects the conductivity of the diamond composites.

**3.2. Electrochemical Behavior of the Metal−Diamond Composites.** Figure 4 shows cyclic voltammograms of the pure oxygen-terminated diamond particles (ODP), as well as

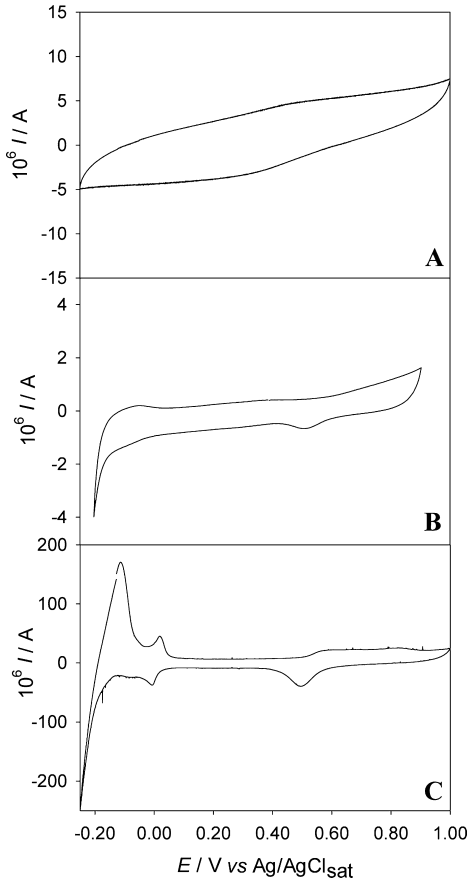


**Figure 4.** Cyclic voltammograms in 0.5 M $H_2SO_4$, at 20 mV $s^{-1}$, of ODP (A), M2-ODP (B), and M1-ODP (C) drop-casted on a glassy carbon electrode.

composites produced by both methods (M1-ODP and M2-ODP), drop-cast on glassy carbon electrodes. ODP shows typical capacitive behavior, with a slight signal around 0.40 V standard for $sp^2$ carbons, likely due to the underlying carbon electrode; previous studies have shown that $sp^2$ impurities in particles are effectively removed during the acid treatment used for the surface oxygenation.[25]

The voltammograms of the metal/diamond composites are dominated by signals characteristic of Pd nanoparticles including responses associated with hydrogen adsorption, absorption, and proton reduction at potentials more negative than 0 V, with the corresponding oxidation and desorption signals upon scan reversal. At potentials more positive than 0.4 V, the voltammetric responses are dominated by Pd oxide formation and reduction. More detailed analyses of the various voltammetric features associated with Pd and core−shell nanostructures have been published elsewhere.[16,22] In general, composites obtained by Method 1 exhibited higher currents and better defined voltammetric features associated with the Pd nanostructures (Figure 4C). The differences in the voltammetric responses between M1-OPD and M2-OPD are mainly linked to the smaller particle size and the higher metal content obtained by Pd impregnation (Method 1). Measurements of the charge associated with the oxidation of a CO monolayer and the reduction of Pd oxide suggest that the specific surface area of the composites obtained by Method 1 is approximately 15 times higher than those obtained by Method 2.

**3.3. Conductivity in Air.** To rationalize the charge transport mechanisms of the various composites, conductance measurements were carried out employing interdigitated electrodes. The right hand side of Figure 5 shows the

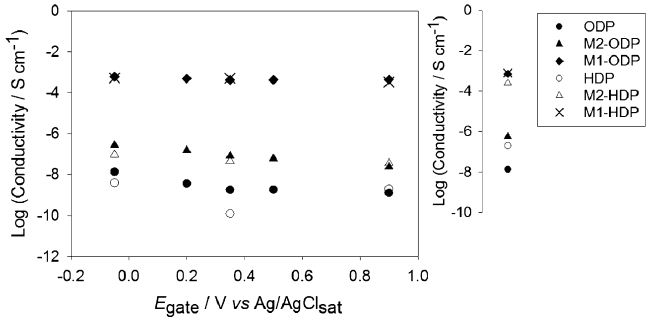


**Figure 5.** Lateral conductivity across the different diamond composites in air (right) and at different gate voltages, while immersed in 0.5 M $H_2SO_4$ (left).

conductivity of each of the diamond composites in air. It can be seen that the conductivity changes by several orders of magnitude depending on both the surface termination of the diamond particles and the presence of metal nanostructures. Although diamond powders contain mainly N impurities, which generate deep trap levels (i.e., nonionizable at room temperature), Figure 5 shows that charge transport is observed on all samples studied. HDP, however, exhibits conductivity more than an order of magnitude higher than ODP in air. This observation can be linked to the so-called *transfer doping model* reported for H-terminated diamond films.[5,9] H-termination induces an upwards shift of the valence band maximum of diamond, leading to surface hole accumulation.

It is also immediately clear that the presence of metal particles increases the conductivity over that of the diamond on its own. Although all metal-containing composites exhibit higher conductivity than pure diamond, there are significant differences between the composites obtained by Method 1 and Method 2. Method 1 leads to similar conductivity on both hydrogen- and oxygen-terminated diamond, while the conductivity of composites prepared using Method 2 is heavily influenced by surface terminations (the conductivity of M2-HDP is more than two orders of magnitude higher than M2-ODP). These observations suggest that there are several charge transfer pathways influencing the conductivity of the composites: (i) charge percolation via metal nanoparticles, (ii) charge transport across the surface of diamond particles (surface conductivity), and (iii) diamond particle-to-particle charge transfer.

As mentioned above, the first noticeable difference is the much higher conductivity obtained for metal-containing composites versus metal-free diamond assemblies. For example, the lateral conductivity of M2-ODP is almost two orders of magnitude higher than ODP, clearly revealing the extent of charge percolation via the metal nanostructures. It has been shown that sufficiently close conducting particles immersed in insulating or semiconducting media can produce charge transport through percolation from one particle to the next.[26−28] The percolation threshold, or minimum distance between particles needed to produce electrical conductivity, decreases with particle size and has been determined theoretically and through experiment to be dependent on the

volume fraction of conducting versus nonconducting parts of the whole.[29−31] The theoretical threshold for a three-dimensional continuum has been calculated as 0.15; essentially macroscopic conductivity of a material is observed when at least 15% of it is conducting.[32] Although an enhanced conductivity with increased metal loading is observed here (e.g., M1-ODP has twice the metal loading of M2-ODP and approximately three orders of magnitude higher conductivity), metal/diamond composites cannot strictly be considered a three-dimensional homogeneous mixture; due to exclusion zones generated for the metal nanostructures by the presence of "hard" diamond particles, percolation pathways could be generated with smaller volume fractions than those predicted for homogeneous three-dimensional continuums. These arguments have been recently demonstrated for grapheme/polystyrene nanocomposites.[33]

As discussed above, H-termination has an effect on the surface conductivity of diamond composites in air; this effect is also seen on metal/diamond composites produced through Method 2. The conductivity of M2-HDP in air is more than two orders of magnitude higher than M2-ODP and HDP, suggesting the contribution of surface conductivity at hydrogenated diamond particles, in addition to charge percolation through the metal nanostructures. M1-ODP and M1-HDP, on the other hand, exhibit essentially the same lateral conductivity in air. Consequently, diamond surface termination does influence the conductivity of the assembly as long as the metal loading is below the percolation threshold mentioned above. Although these results are somewhat expected, conductivity measurements carried out in an electrochemical environment do reveal a rather different scenario.

**3.4. Conductivity in the Presence of Electrolyte Solution.** Figure 5 also shows the conductivity as a function of gate voltage, in an electrochemical environment. Although a small decrease with increasingly positive potentials is observed in all cases, there is little dependence of the conductivity $E_{gate}$. The $E_{gate}$ range was confined to the region where no faradaic reaction takes place, although regions in which Pd is covered by hydrogen and oxygen are included. These surface processes at the metal nanoparticles do not affect the charge transport properties of the composites. The trend in conductivity Method 1 > Method 2 > metal-free composites observed in air is maintained in aqueous electrolyte, at all potentials, confirming the importance of percolation pathways through the metal nanostructures in the conductivity of the samples.

An interesting trend in Figure 5 is the similar conductivity observed in the electrochemical environment for HDP and ODP assemblies in the absence of metal nanoparticles. *This result indicates that the intrinsic surface conductivity of the hydrogenated diamond surface does not play a significant role in charge transport in the presence of electrolyte solutions.* It is important to note that this was not caused by irreversible loss of the hydrogen termination in electrochemical conditions; conductivity of dry samples, in air, was measured both before and after experiments in electrolyte, producing identical results. This observation suggests that the ubiquitous formation of the electrochemical double layer at the composite/electrolyte interface decreases charge transport. The presence of a liquid with ionic charge carriers screens electron−electron repulsions present in semiconducting assemblies. Carriers at the surface are paired with inert ions in solution, compensating electronic charges; this process has an effect on tunneling barriers and consequently on charge mobility.[12] It has been found that small changes in the tunneling barriers due to, for example, adsorption processes or changes in the solvent used can have measurable effects on long-range mobility of charge carriers across semiconducting assemblies.[12,33]

The effect of the electrolyte solution on the diamond composites is qualitatively different from previous investigations on continuous diamond films,[21,34,35] due to the dominant role of particle-to-particle charge transfer. In view of the results shown in Figure 5, it can be concluded that charge percolation through the metal nanostructures and via the diamond surface plays a role in composite conductivity, depending on the volume ratio of the metal. In samples with volume ratios above 12%, charge transport is fully dominated by percolation through the metal nanostructures, with very little effect from ionic species in solution or diamond surface termination. Indeed, the fact that the conductivity in air and in electrochemical environment is essentially identical in impregnated composites (Method 1) confirms that the contribution of the diamond particles to the charge transport is negligible. For lower volume ratios and metal-free assemblies, the surface conductivity of the diamond particles plays an important role in air. However, interparticle charge transfer is severely affected by the presence of electrolyte species in solution, reducing the overall conductivity of surface-hydrogenated particles. These observations have important consequences in the formulation of metal/diamond composites for applications in sensor and electrocatalysis. For instance, Swain and co-workers have recently developed a method of coating diamond nanoparticles with an ultrathin layer of boron-doped diamond, which shows high surface area and very high conductivity in air.[36] There is no doubt that this approach would lead to high conductivity in an electrolytic environment; however, the ionic environment could also affect charge transport between diamond particles. In addition to diamond conductivity, other parameters that could determine the suitability of these powders as support for application in electrocatalysis include the diamond particle size and alternative particle binders. These aspects are currently under investigation.

## 4. CONCLUSIONS

Lateral conductivity of composites featuring metal nanostructures and diamond particles has been investigated in air and in electrolyte solutions employing electrochemical field-effect transistors. The charge transport properties of the composite were investigated as a function of the metal loading, diamond surface termination, and the electrochemical potential of the diamond composite (gate voltage). It was observed that the conductivity in composites with metal volume fractions above 12% is dominated by percolation pathways through the metal nanostructures, which are ca. 50 times smaller than the mean diamond size. This limit approaches the theoretical 15% established from percolation theory.

Composites with metal volume fractions below 12% have a more complex behavior, which is dependent on the hydrogen surface termination and the presence of ionic species in solution. In air, H-terminated diamond particles exhibit higher overall conductivities than equivalent O-terminated samples. However, this enhancement is lost upon immersion in aqueous electrolyte, where not only do hydrogen- and oxygen-terminated samples produce similar conductivity values but also both are lower than those obtained in air. These observations clearly show that information obtained from conventional conductance measurements in air may not be directly applicable to composites in electrolyte solution.

## AUTHOR INFORMATION


### Corresponding Author

*E-mail: david.fermin@bristol.ac.uk. Fax: +44 117 927-7985.


### Notes

The authors declare no competing financial interest.

## ACKNOWLEDGMENTS

The authors acknowledge A. Moore, Dr. M. G. Montes de Oca, Dr. W. Hongthani, and Dr. N. Fox (University of Bristol) for their contributions to this work. We also thank J. A. Jones (University of Bristol) for his support with the characterization of nanostructures by Electron Microscopy. We thank the EPSRC (project EP/H046305/1) and the University of Bristol for financial support.

## REFERENCES


(1) Turova, O. V.; Starodubtseva, E. V.; Vinogradov, M. G.; Sokolov, V. I.; Abramova, N. V.; Vul, A. Y.; Alexenskiy, A. E. *Catal. Commun.* **2011**, *12*, 577−579.

(2) Nakagawa, K.; Kikuchi, M.; Nishitani-Gamo, M.; Oda, H.; Ganto, H.; Ogawa, K.; Ando, T. *Energy Fuels* **2008**, *22*, 3566−3570.

(3) Yasu-eda, T.; Se-ike, R.; Ikenaga, N.-o.; Miyake, T.; Suzuki, T. *J. Mol. Catal. A: Chem.* **2009**, *306*, 136−142.

(4) Holt, K. B.; Ziegler, C.; Zang, J.; Hu, J.; Foord, J. S. *J. Phys. Chem. C* **2009**, *113*, 2761−2770.

(5) Maier, F.; Riedel, M.; Mantel, B.; Ristein, J.; Ley, L. *Phys. Rev. Lett.* **2000**, *85*, 3472−3475.

(6) Holt, K. B. *Phys. Chem. Chem. Phys.* **2010**, *12*, 2048−2058.

(7) Hongthani, W.; Fox, N. A.; Fermin, D. J. *Langmuir* **2011**, *27*, 5112−5118.

(8) Garrido, J. A.; Nowy, S.; Haertl, A.; Stutzmann, M. *Langmuir* **2008**, *24*, 3897−3904.

(9) Haertl, A.; Garrido, J. A.; Nowy, S.; Zimmermann, R.; Werner, C.; Horinek, D.; Netz, R.; Stutzmann, M. *J. Am. Chem. Soc.* **2007**, *129*, 1287−1292.

(10) Compton, R. G.; Foord, J. S.; Marken, F. *Electroanalysis* **2003**, *15*, 1349−1363.

(11) Krueger, A.; Lang, D. *Adv. Funct. Mater.* **2012**, *22*, 890−906.

(12) Wang, X. F.; Ishii, Y.; Ruslinda, A. R.; Hasegawa, M.; Kawarada, H. *ACS Appl. Mater. Interfaces* **2012**, *4*, 3526−3534.

(13) Hutton, L. A.; Vidotti, M.; Patel, A. N.; Newton, M. E.; Unwin, P. R.; Macpherson, J. V. *J. Phys. Chem. C* **2011**, *115*, 1649−1658.

(14) Iniesta, J.; Michaud, P. A.; Panizza, M.; Cerisola, G.; Aldaz, A.; Comninellis, C. *Electrochim. Acta* **2001**, *46*, 3573−3578.

(15) Awada, H.; Strojek, J. W.; Swain, G. M. *J. Electrochem. Soc.* **1995**, *142*, L42−L45.

(16) Moore, A.; Celorrio, V.; de Oca, M. M.; Plana, D.; Hongthani, W.; Lazaro, M. J.; Fermin, D. J. *Chem. Commun.* **2011**, *47*, 7656−7658.

(17) La-Torre-Riveros, L.; Guzman-Bas, R.; Mendez-Torres, A. E.; Prelas, M.; Tryk, D. A.; Cabrera, C. R. *ACS Appl. Mater. Interfaces* **2012**, *4*, 1134−1147.

(18) Bian, L. Y.; Wang, Y. H.; Zang, J. B.; Meng, F. W.; Zhao, Y. L. *Int. J. Hydrogen Energy* **2012**, *37*, 1220−1225.

(19) Sharma, S.; Pollet, B. G. *J. Power Sources* **2012**, *208*, 96−119.

(20) Roest, A. L.; Kelly, J. J.; Vanmaekelbergh, D.; Meulenkamp, E. A. *Phys. Rev. Lett.* **2002**, *89*, 036801−036801.

(21) Garrido, J. A.; Hartl, A.; Dankerl, M.; Reitinger, A.; Eickhoff, M.; Helwig, A.; Mueller, G.; Stutzmann, M. *J. Am. Chem. Soc.* **2008**, *130*, 4177−4181.

(22) de Oca, M. G. M.; Kurnarakuru, H.; Cherns, D.; Fermin, D. J. *J. Phys. Chem. C* **2011**, *115*, 10489−10496.

(23) de Oca, M. G. M.; Plana, D.; Celorrio, V.; Lazaro, M. J.; Fermin, D. J. *J. Phys. Chem. C* **2012**, *116*, 692−699.

(24) Celorrio, V.; de Oca, M. G. M.; Plana, D.; Moliner, R.; Lazaro, M. J.; Fermin, D. J. *J. Phys. Chem. C* **2012**, *116*, 6275−6282.

(25) Hongthani, W.; Fermin, D. J. *Diamond Relat. Mater.* **2010**, *19*, 680−684.

(26) Last, B. J.; Thouless, D. J. *Phys. Rev. Lett.* **1971**, *27*, 1719.

(27) Muller, K. H.; Wei, G.; Raguse, B.; Myers, J. *Phys. Rev. B: Condens. Matter Mater. Phys.* **2003**, *68*, 155407.

(28) Schmelzer, J.; Brown, S. A.; Wurl, A.; Hyslop, M.; Blaikie, R. J. *Phys. Rev. Lett.* **2002**, *88*, 226802.

(29) Jing, X.; Zhao, W.; Lan, L. *J. Mater. Sci. Lett.* **2000**, *19*, 377−379.

(30) Yoshida, K.; Tomii, Y.; Ueda, S. *Jpn. J. Appl. Phys., Part 1* **1988**, *27*, 2224−2226.

(31) Dubson, M. A.; Garland, J. C. *Phys. Rev. B: Condens. Matter Mater. Phys.* **1985**, *32*, 7621−7623.

(32) Scher, H.; Zallen, R. *J. Chem. Phys.* **1970**, *53*, 3759−3761.

(33) Qi, X.-Y.; Yan, D.; Jiang, Z.; Cao, Y.-K.; Yu, Z.-Z.; Yavari, F.; Koratkar, N. *ACS Appl. Mater. Interfaces* **2011**, *3*, 3130−3133.

(34) Szameitat, M.; Jiang, X.; Beyer, W. *Appl. Phys. Lett.* **2000**, *77*, 1554−1556.

(35) Nebel, C. E.; Kato, H.; Rezek, B.; Shin, D.; Takeuchi, D.; Watanabe, H.; Yamamoto, T. *Diamond Relat. Mater.* **2006**, *15*, 264−268.

(36) Guo, L.; Swope, V. M.; Merzougui, B.; Protsailo, L.; Shao, M.; Yuan, Q.; Swain, G. M. *J. Electrochem. Soc.* **2010**, *157*, A19−A25.